Letter

Chinese Science Bulletin

Geology

November 2011 Vol.56 No.31: 3273–3280
doi: 10.1007/s11434-011-4680-z

Surface latent heat flux anomalies before the M_S 7.1 New Zealand earthquake 2010

QIN Kai[1], WU LiXin[2*], DE SANTIS Angelo[3] & WANG He[1]

[1] *College of Geosciences and Surveying Engineering, China University of Mining and Technology (Beijing), Beijing 100083, China;*
[2] *Key Laboratory of Environment Change and Natural Disaster (Ministry of Education), Beijing Normal University, Beijing 100875, China;*
[3] *Istituto Nazionale di Geofisica e Vulcanologia, Rome 00143, Italy*

Received April 28, 2011; accepted July 7, 2011; published online August 30, 2011

By analyzing surface latent heat flux (SLHF) data from the NCEP/NCAR Reanalysis Project for the period three months before and after the Sept. 3, 2010 M_S 7.1 New Zealand earthquake, an isolated SLHF positive anomaly on Aug. 1, 2010 was found with a high value of about 160 W/m^2 to the northeast of the epicenter. Historical data, background pixels, and wavelet transforms of time series were comprehensively analyzed to study the spatiotemporal features of the SLHF anomaly. After removing the influences of wind speed and cloud cover, the key factor leading to local SLHF anomalies is the surface temperature increment. Combined with GPS displacement observations and tectonic settings, we determined that the physical mechanism of the SLHF anomaly could possibly be attributed to hot underground materials related to high-temperature and high-pressure upwelling from the deep crust and mantle along the nearby subduction zone, thereby explaining the local temperature increment to the northeast of the epicenter, as well as in the center of the North Island and the southwest of the South Island. Furthermore, it changed the specific humidity between the ground and surface air, causing the local SLHF increment.

New Zealand earthquake, surface latent heat flux, surface temperature, anomaly, displacement

Citation: Qin K, Wu L X, De Santis A, et al. Surface latent heat flux anomalies before the M_S 7.1 New Zealand earthquake 2010. Chinese Sci Bull, 2011, 56: 3273–3280, doi: 10.1007/s11434-011-4680-z

In 2003, Dey and Singh were the first to report surface latent heat flux (SLHF) anomalies before a large coastal earthquake [1]. Chen et al. [2] and Singh et al. [3] then further analyzed SLHF anomalies before the 2004 M_S 9.0 Indonesia earthquake. Later, Li et al. [4] and Qin et al. [5,6] revealed that abnormal SLHF also occurred before inland earthquakes and showed that the spatial patterns of such anomalies have good correspondence with the direction of local active faults. In addition, Cervone et al. [7] developed a wavelet analysis approach to identify the maximum peaks of SLHF associated with an impending earthquake and demonstrated a link with atmospheric disturbances. Nikitas et al. [8] discussed the multi-fractal characteristics of SLHF time series and its significance in earthquake monitoring and early warning. According to the New Zealand GNS Science (www.geonet.org.nz), a M_S 7.1 earthquake happened on the South Island of New Zealand (43.52°S, 172.17°E) at 16∶35 UTC on Sept. 3, 2010 (04∶35 local time on Sept. 4, 2010), with a focal depth of 10 km. By analyzing the spatial distribution of SLHF three months before and after the earthquake, the authors found that there was an obvious positive SLHF anomaly to the northeast of the epicenter about a month before the event. To confirm the association of the SLHF anomaly with the earthquake, historical data, background pixels, time series and influencing factors have been comprehensively analyzed and checked.

The SLHF and surface temperature dataset used in the paper are the daily mean values from NCEP/NCAR Reanalysis Project, which is a joint project of the National Centers for Environmental Prediction (NCEP) and the National Center for Atmospheric Research (NCAR). The dataset is generated from multi-source observations such as land surface,

*Corresponding author (email: awulixin@263.net)

ship, rawinsonde, pibal, aircraft, satellite, and other sensors. These data were then quality controlled and assimilated using a system that was kept unchanged over the reanalysis period. The data are represented by a Gaussian grid of 94 lines from the equator to the pole, with a regular 1.875° longitudinal spacing.

First, the spatial distribution of SLHF over a large region (165°–180°E, 34°–48°S) around the epicenter was analyzed for the period Jul. 1 to Sept. 30, 2010. The results show a spot-shaped anomaly with a high value of about 160 W/m^2 to the northeast of the epicenter on Aug. 1, 2010 (Figure 1). Data from the corresponding period in the non-earthquake years of 2008 and 2009 were chosen for comparison and especially to investigate the association of the anomaly with the seismogenic process of the New Zealand earthquake (Figure 2a and b). We found that the spatial distribution of SLHF is generally higher in the north and lower in the south in accordance with the difference of latitude on Aug. 1, 2008, and is higher in the east and lower in the west bounded by New Zealand on Aug. 1, 2009. The spatial distribution of SLHF for the same periods in 2008 and 2009 was mainly controlled by geographic and meteorological factors, but no anomaly similar to the one that appeared on Aug. 1, 2010 was seen. We then subtracted the mean value of a range of non-shock years (1990–2009), representing a background, from the SLHF data from 2010 to obtain an SLHF increment (ΔSLHF) (Figure 2c). Similar to the spatial distribution of SLHF, the spatial distribution of ΔSLHF on Aug. 1, 2010 also showed a spot-shaped anomaly to the northeast of the epicenter. In addition, two weaker anomalies were observed in the central North Island and the southwest South Island. These small SLHF anomalies may, in fact, be spatially precursory features. This then poses a question regarding the distribution of SLHF features in this region during non-shock periods.

For this purpose, long time series SLHF datasets were analyzed. As the SLHF anomaly caused by the earthquake should be confined to the vicinity of the epicenter and the particular tectonic area, we chose a pixel far away from the seismic zone (at 44.7611°S, 170.625°E, labeled 2 in Figures 1 and 2) as the normal background, and compared it with the epicenter pixel (at 42.8564°S, 172.5°E, labeled 1 in Figures 1 and 2). Intuitive analysis shows that the SLHF annual variation curve of the non-shock pixel (Figure 3a)

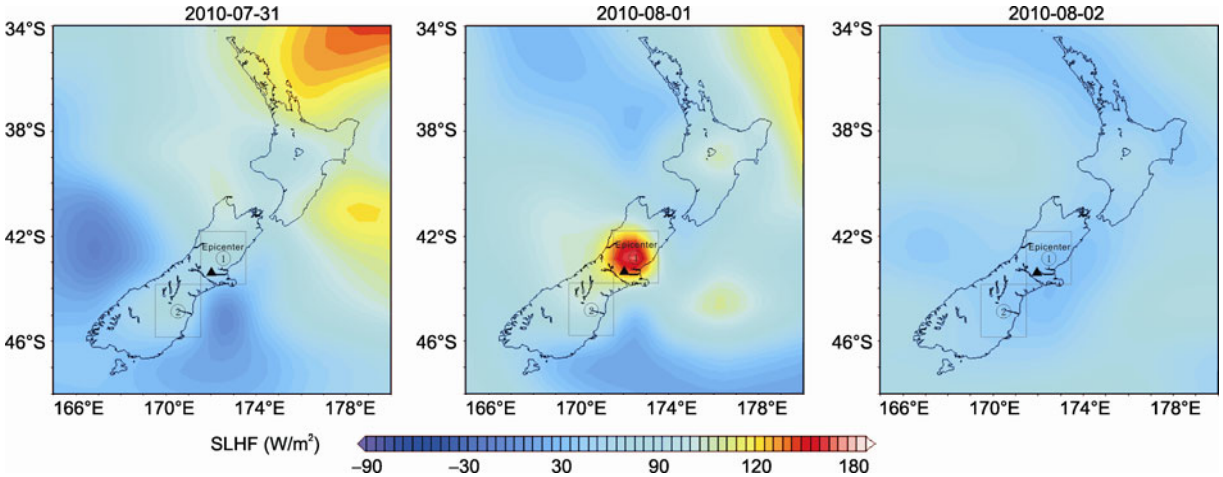

Figure 1 Spatial distributions of SLHF from Jul. 31 to Aug. 2, 2010.

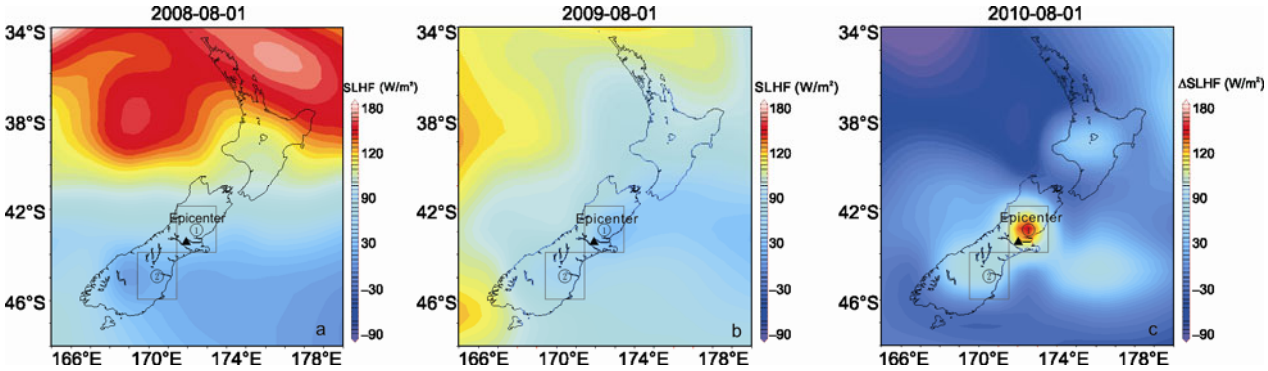

Figure 2 Spatial distribution of SLHF (a, b) and spatial distribution of ΔSLHF (c).

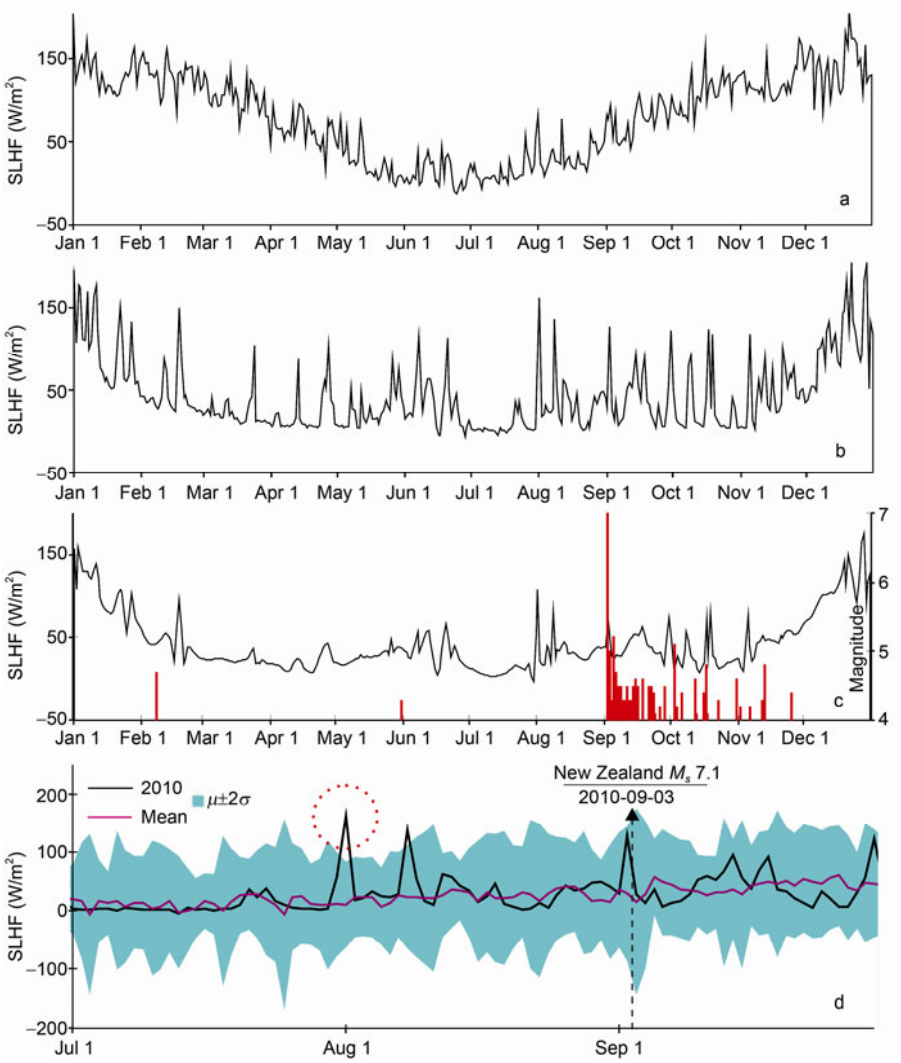

Figure 3 Temporal features of SLHF. a, SLHF annual time series of pixel 2 in 2010; b, SLHF annual time series of pixel-1 in 2010; c, SLHF annual time series of pixel-1 in 2010 after wavelet-transformation and reconstruction, and the magnitude time series of the earthquakes in pixel-1; d, SLHF time series of pixel-1 from Jul. 1 to Sept. 30, 2010, and its comparison with historical data over the same period. The black line is the SLHF variation curve of 2010, the pink line is the mean (μ) variation curve on the same day during the non-shock years (1990–2009), the blue zone is the multi-year mean value plus or minus twice the standard deviation (σ) (i.e. inferred noise), and the arrows indicate the earthquake time.

appears to be a series of trigonometric curves with noise, having a maximum in January and December (austral summer) and a minimum in July (austral winter). In comparison, the SLHF annual variation curve of the epicenter pixel is disordered, which can be interpreted to be the result of information superposition from such sources as seasons, tides, rain clouds, cold-or-hot air currents, or seismotectonic activity (Figure 3b). The paroxysmal signal associated with the seismotectonic activity may be extracted from this detailed SLHF annual variation curve using computing functions such as wavelet transform dilations and translations [9,10].

First, the SLHF annual variation curve of the epicenter pixel was decomposed (the decomposition number is 5) by an orthogonal Coiflet wavelet with good symmetry and compact support. Second, a reconstructed SLHF annual variation curve (Figure 3c) was obtained by superimposing the decomposed approximation coefficients and the detailed coefficients. The results show that interference signals, such as tides, rain clouds, or cold-or-hot air currents, have been essentially removed from the SLHF signal after wavelet noise reduction. Seasonal characteristics are clearly revealed in addition to records of obvious seismotectonic activity. Investigation of the earthquake magnitude time series from 2010 for the epicenter pixel permits us to infer that the peaks of SLHF in February and May are possibly associated with M_S 4.7 and M_S 4.3 earthquakes on Feb. 9 and Jun. 1, 2010, respectively (as coseismic effects or precursory anomalies); the peak on Aug. 1, the highest for the whole year, appears to be in a good precursory relationship with the M_S 7.1 event on Sept. 3, 2010. Several peaks following the earthquake are possibly associated with aftershocks.

To obtain high-resolution temporal features of the SLHF annual variation curves from the epicenter pixel (Figure 3d), daily SLHF data from Jul. 1 to Sept. 30 of each year from 1990–2010 were analyzed. We discovered that the SLHF readily exceeded the upper limit of the noise on Aug. 1, suddenly increasing from 56.7 W/m^2 on Jul. 31 to 162 W/m^2 on Aug. 1, then returning to the mean value on Aug. 8, and increasing again the day before the earthquake, Sept. 2, albeit still below the upper noise limit.

The comprehensive analysis above shows that the SLHF anomalies to the northeast of the epicenter, and the two weak SLHF anomalies in the central North Island and southwestern South Island on Aug. 1, 2010, all of which are higher than the normal historical background levels and different from wide-area meteorological effects, should be considered precursory anomalies closely related to the M_S 7.1 New Zealand earthquake. Assuming this is the case, then what are the physical factors leading to the anomalies? It is well known that SLHF can reflect water and heat exchange between the ground surface and the atmosphere, as a result of the heat absorbed or released by phase transitions (condensation, evaporation or melting) of atmospheric moisture, and affected by many factors such as air humidity, wind speed and surface temperature. Its bulk aerodynamic formulation can be written as [11]:

$$\mathrm{SLHF} = \rho L_e c_e U(q_s - q_a) = \rho L_e c_e U \Delta q, \quad (1)$$

where ρ and L_e are constants, c_e denotes the bulk transfer coefficient, U is the wind speed, the subscript a corresponds to a reference altitude, s denotes surface quantities, and q is the specific humidity; Δq is the difference between q_s and q_a, which is a function of surface temperature and can be expressed as

$$\Delta q = q_s(T_s) - q_a(T_s + \Delta T), \quad (2)$$

where T_s is surface temperature and ΔT is the difference between surface temperature and air temperature.

Admittedly, the primary factors affecting SLHF are wind speed and surface temperature. However, the effect of wind speed on SLHF should be a wide-area meteorological effect rather than a local one. By analyzing the surface temperature increment (ΔT_s) compared with the mean value for non-shock years (1990–2009), we found that local high-temperature anomalies of 3°–6°C had appeared both in the strong SLHF anomaly zone and in the two weak SLHF anomaly zones on July 31 and Aug. 1, 2010 (Figure 4). Therefore, the key factor leading to the SLHF anomalies might be surface temperature rather than wind speed. With an infrared satellite cloud map of FY-2D (Figure 5) and weather station observations from the area (Table 1), we ascertained that conditions were mainly sunny with sporadic haze distributions and low-speed relatively-stable winds. This shows that the local high-temperature anomalies on Jul. 31 and Aug. 1 resulted neither from solar radiation enhancement of the reduced cloud (e.g. cloudy to clear), nor from a warm air mass effects, but rather most likely resulted from underground heat.

Using continuous GPS observation data in the International Terrestrial Reference Frame (ITRF) provided by New Zealand GeoNet Project (http://www.geonet.org.nz/), we calculated the daily displacement of each station compared with the previous day from Jul. 1 to Sept. 30, 2010, and determined the time series of the displacement components of GPS stations (Figure 6). A displacement anomaly index, reflecting the displacement fluctuation, was then determined by subtracting the mean value of daily displacements from the daily displacement of each station, and dividing by the standard deviation (Figure 7). Accordingly, it was found that the N-S displacement components of GPS stations (HAAS, LEXA, KAIK, WITH, NLSN and KARA) in New

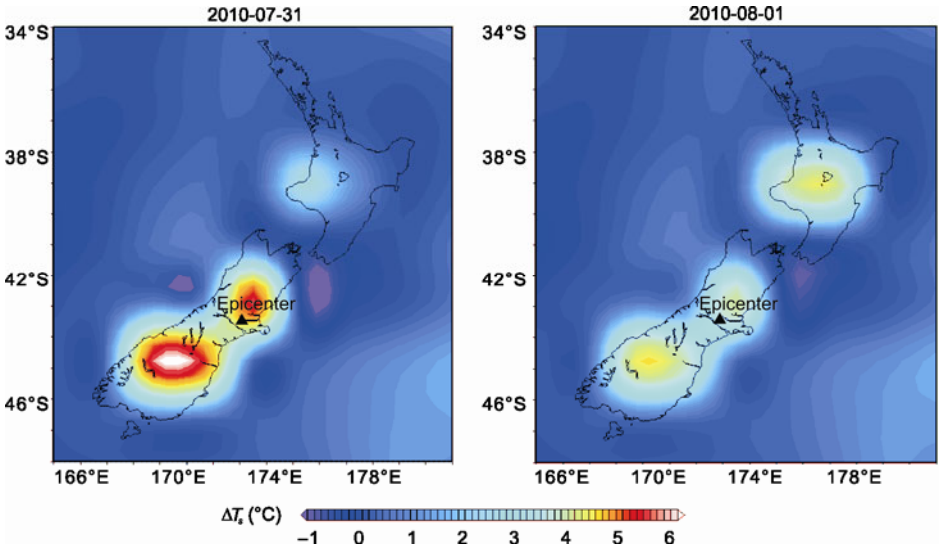

Figure 4 Spatial distribution of ΔT_s on Jul. 31 and Aug. 1, 2010.

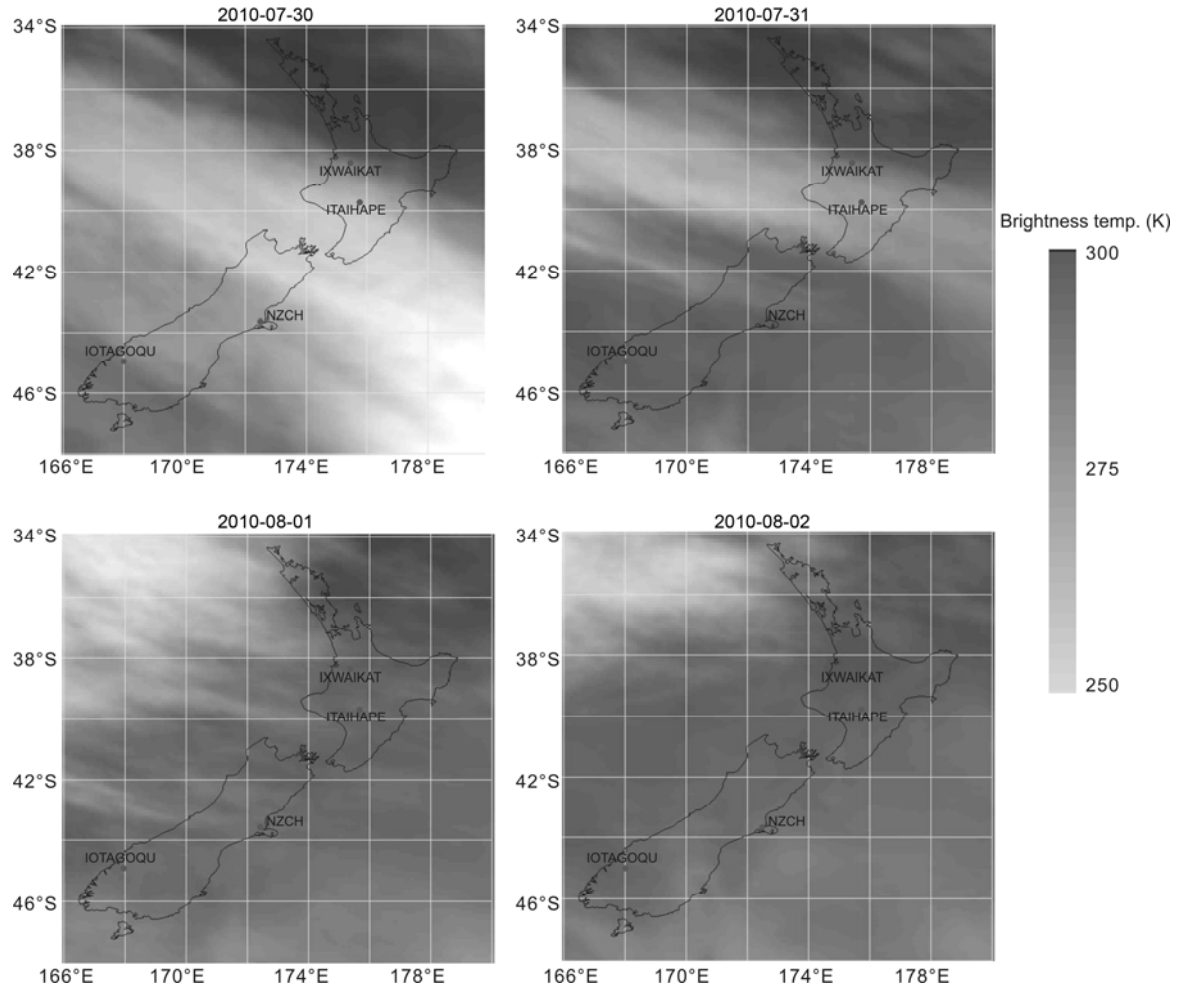

Figure 5 Infrared cloud maps from Fy-2D from Jul. 30 to Aug. 2, 2010.

Table 1 Observations of the weather stations near the temperature increasing area (null values indicate missing data)

Station	Date	Time	Wind speed (m/s)	Condition	Station	Date	Time	Wind speed (m/s)	Condition
IOTAGOQU	2010-07-31	00:00	0.53	cloud	NZCH	2010-07-31	00:00		
		06:00	2.01	cloud			06:00	2.89	cloud
		12:00	2.06	cloud			12:00	1.28	partly cloudy
		18:00	1.53	cloud			18:00	0.64	partly cloudy
	2010-08-01	00:00	1.53	cloud		2010-08-01	00:00		
		06:00	3.08	cloud			06:00	1.28	cloud
		12:00	1.78	cloud			12:00	2.56	cloud
		18:00		rain			18:00	5.11	cloud
IXWAIKAT	2010-07-31	00:00	1.03	cloud	ITAIHAPE	2010-07-31	00:00	0.44	cloud
		06:00		cloud			06:00	3.14	cloud
		12:00		cloud			12:00	0.89	cloud
		18:00	1.03	cloud			18:00	4.47	cloud
	2010-08-01	00:00	1.56	rain		2010-08-01	00:00	11.61	cloud
		06:00	1.03	cloud			06:00	9.39	
		12:00	1.03	cloud			12:00	2.22	cloud
		18:00	0.5	cloud			18:00	3.58	cloud

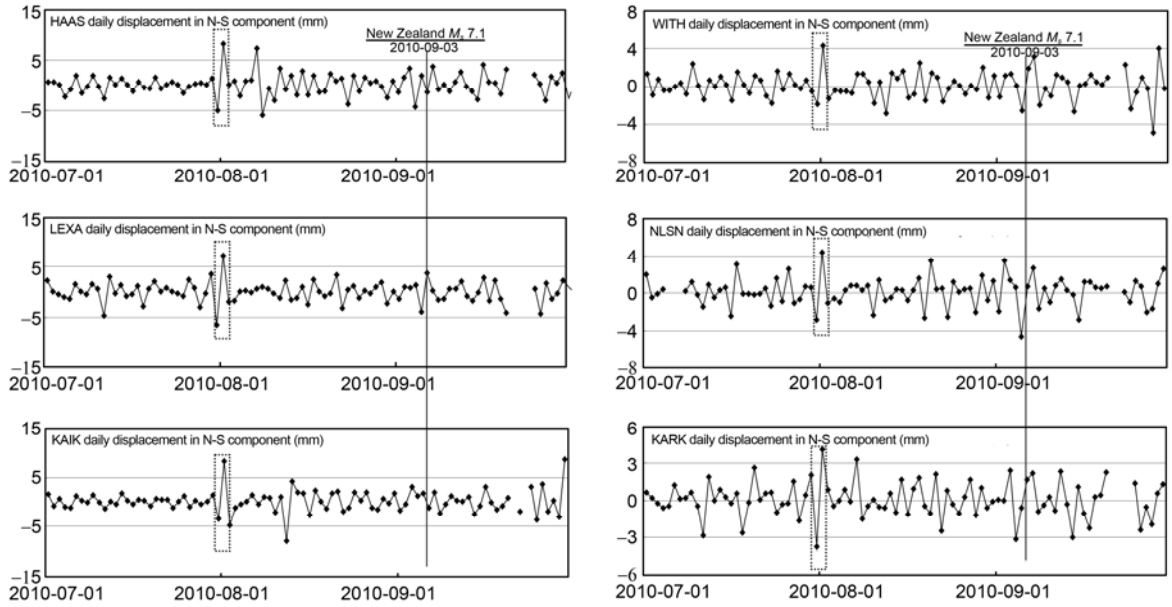

Figure 6 Time series of GPS displacement components (data from New Zealand GeoNet project).

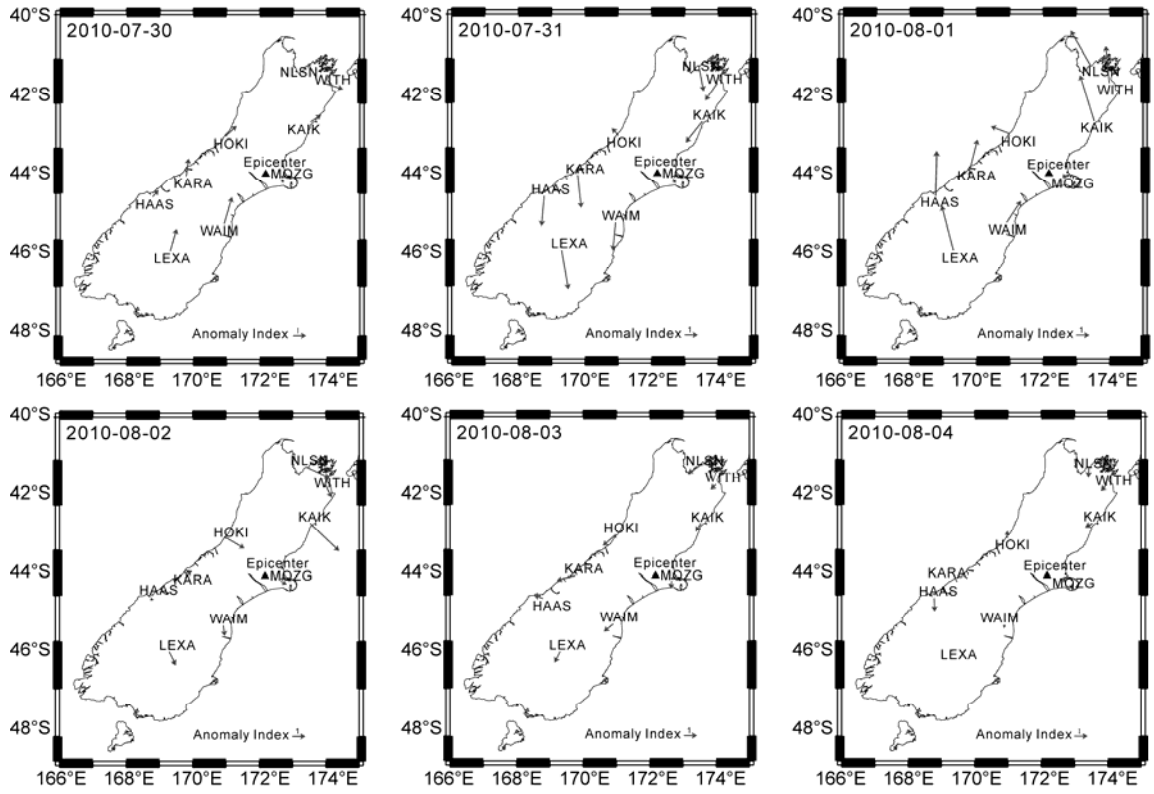

Figure 7 Anomaly index map of GPS displacement (data from New Zealand GeoNet project).

Zealand recorded a quasi-synchronous fluctuation on Jul. 31 and Aug. 1 2010. This is consistent with the time of the surface temperature anomalies, and reflects tectonic activity enhancement before the earthquake.

In contrast with previous earthquake cases [1–6], the SLHF anomaly before the M_S 7.1 New Zealand earthquake occurred mainly as a small isolated temporally-limited "hot spot" patch but not moved along significant tectonic structures. Its position may be associated with the particular tectonic setting of New Zealand. As shown in Figure 8, New Zealand is located on the tectonic plate boundary between the Australian and Pacific plates. The oblique collision of

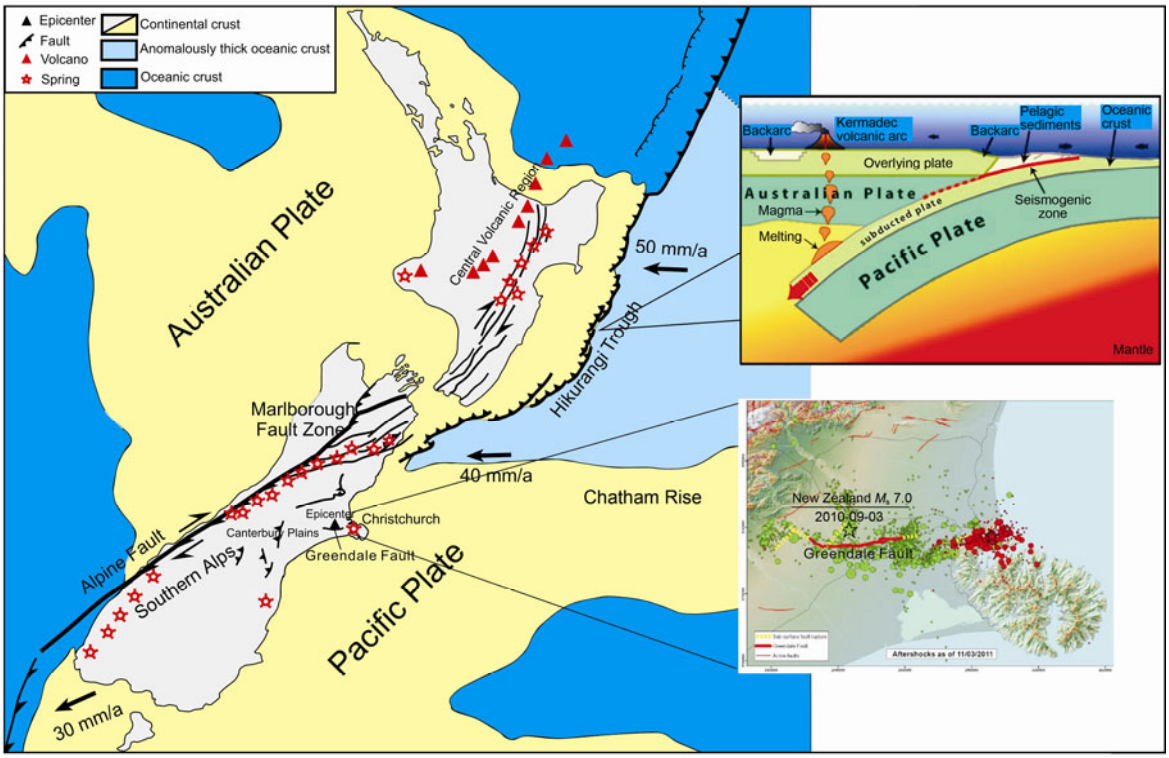

Figure 8 Tectonic map in the seismic region of M_S 7.1 New Zealand EQ (Provided by Prof. Jarg Pettinga, University of Canterbury).

the two plates causes the Pacific Plate to subduct beneath the Australian Plate, which forms a high-temperature and high-pressure zone in the lithosphere. The subduction process provides sufficient energy for hot material to upwell from mantle, which leads to abundant geothermal activity such as hot springs and volcanoes [12]. The SLHF anomalies before the earthquake are located in the Marlborough fault zone to the northeast of the epicenter, in the volcanic zone at the center of the North Island, and in the Southern Alps with many hot springs. According to post-earthquake reports, the M_S 7.1 New Zealand earthquake was caused by a 'new' fault named the Greendale Fault in the Canterbury Plains, which is at the southern leading edge of the Marlborough fault system. Based on GPS, geological and seismological data, Wallace et al. [13] analyzed the active deformation in the South Island of New Zealand. They found that the Chatham Rise is migrating southwest along the New Zealand plate boundary (relative to the Australian Plate) at 28–37 mm/a, and that the Hikurangi Plateau permits southward propagation of the Hikurangi subduction zone in relation to the Australian Plate. The possible driving mechanisms could be mantle movement beneath the region [13].

Therefore, the physical mechanism of the SLHF anomalies before the M_S 7.1 New Zealand earthquake can be interpreted. First, the long-term tectonic activity in the interface region between the Pacific and Australian plates was enhanced in the latter period of the seismogenic process, leading to rock expansion and crack propagation in the local subduction zone and hence providing abundant channels for hot material upwelling from the deep crust and mantle. Second, hot material resulted in the gradual expansion of the region and then caused local temperatures to increase in particular zones (the geothermal areas northeast of the epicenter, at the center of the North Island and in the southwestern South Island), which are connected with subsurface fluids. Third, the surface temperature increment affected change in the difference between the specific humidity of the ground and the overlying surface air masses, hence resulting in local SLHF increases. The above discussion is just our initial interpretation. Further studies should be undertaken to investigate the lithosphere-coversphere atmosphere (LCA) coupling effect [14]. Correlative analysis on multi-parameter anomalies will be essential to fully explain the mechanisms behind the SLHF anomaly and precursive features.

Surface latent heat flux and surface temperature data came from the NCEP/NCAR Reanalysis Project. The satellite cloud map came from the China National Meteorology Centre. Weather Observation Station data came from the Weather Underground website, and GPS data came from the New Zealand GeoNet project. We have discussed this work with experts from the China National Meteorological Information Centre and the University of Canterbury. Two anonymous reviewers have made critical reasonable revision comments and modified the manuscript, respectively. We greatly appreciate their help. This work was supported by the National Basic Research Program of China (2011CB707102), the Fundamental Research Funds for the Central Universities (2010YD01) and the Program of Scientific and Technological Cooperation Between Italy and China (SAGA-4-EPR).

1 Dey S, Singh R P. Nat Hazards Earth Sys, 2003, 3: 749–755
2 Chen M H, Deng Z H, Yang Z Z, et al. Chinese Sci Bull, 2005, 51: 1010–1013
3 Singh R P, Cervone G, Kafatos M, et al. Int J Remote Sensing, 2007, 31: 2885–2896
4 Li J P, Wu L X, Wen Z Y, et al. Sci Tech Rev, 2008, 26: 40–44
5 Qin K, Guo G M, Wu L X. Earthq Sci 2009, 22: 555–562
6 Qin K, Wu L X, Ma W Y. Sci Tech Rev, 2010, 28: 68–73
7 Cervone G, Singh R P, Kafatos M, et al. Nat Hazards Earth Syst Sci, 2005, 5: 87–99
8 Nikitas P, Guido C, Fotini P, et al. Physica A, 2006, 371: 703–718
9 Chen S Y, Liu P X, Liu L Q, et al. Chin J Geophys, 2006, 49: 824–830
10 Zhang Y S, Guo X, Zhong M J, et al. Chinese Sci Bull, 2010, 55: 1917–1924
11 Liu W T, Katsaros K B, Businger J A. J Atmos Sci, 1979, 36: 1722–1735
12 Shi Y L, Fan T Y. Chin J Geophys, 2001, 44: 754–760
13 Wallace L M, Beavan J, McCaffrey R, et al. Geophys J Int, 2007, 168: 332–352
14 Wu L X, Liu S J. Advances in Geosciences & Remote Sensing. Sweden: In-Teh, 2009. 709–741